Interactions between coarse and fine galena and quartz particles and their implications for flotation in NaCl solutions

Anna M. Nowosielska†, Aleksandar N. Nikoloski† and Drew F. Parsons*‡

†College of Science, Health, Engineering and Education, Murdoch University, 90 South St, Murdoch, WA 6150, ***Australia***

‡Department of Chemical and Geological Sciences, University of Cagliari, Cittadella Universitaria, 09042 Monserrato, CA, ***Italy***

Keywords: Flotation, Galena, Quartz, Chemisorption, Interaction Free Energy

Main findings:

- The recovery of galena improves for higher NaCl concentrations.
- Highest recovery for Coarse galena/Coarse quartz (CC) particle system, and the lowest for Fine galena/Fine quartz (FF) particle system.
- Higher recovery reported for Fine galena/Coarse quartz (FC) particle system compared to Coarse galena/Fine quartz (CF) particle system.
- Recovery driven by a stronger attraction of air bubbles towards the galena particles whilst the quartz/air bubble interactions indicate repulsion.

*Electronic mail: drew.parsons@unica.it

ABSTRACT

In this study we have investigated the interactions between coarse and fine galena and quartz particles and their implications for flotation in NaCl solutions. Tested were four different particle systems: (CC) Coarse galena/Coarse quartz, (CF) Coarse galena/Fine quartz, (FC) Fine galena/Coarse quartz and (FF) Fine galena/Fine quartz. The flotation experiments were carried out on the four particle systems in NaCl concentrations of 10 mM and 100 mM, at pH 9. It was found that the recovery was the highest for the CC particle system, and the lowest for the FF particle system. The experiments also indicated that the recovery improved for the higher NaCl concentration.

As part of this study, we calculated the total interaction free energy as a function of separation distance for each pairwise combination of particles and bubbles, for each test condition. It was found that for all particle systems, galena/quartz interactions are dominated by repulsion. The interactions between two galena particles indicated attraction as the dominating force, while the interactions between quartz particles showed repulsion in 10 mM NaCl, which changed to attraction with an increase in NaCl concentration. Galena/air bubble interactions were controlled by repulsive electrostatic interactions in 10 mM NaCl, but these interactions became attractive in 100 mM NaCl salt solutions. On the other hand, the quartz/air bubble interactions were always repulsive, irrespective of the NaCl concentration. Based on these theoretical predictions, we postulate that the stronger repulsion of quartz particles towards the air bubbles could be the driving force for galena recovery.

1. Introduction

In mineral processing, froth flotation is a widely used method for separating target mineral particles from the gangue particles when both are mixed in an aqueous pulp. The efficiency of the process depends mainly on the number of successful particle-bubble collisions that lead to the formation of stable particle-bubble aggregates, recoverable in the froth layer (Leistner et al.,2017).

Mineral processing involving froth flotation requires large amounts of water and with shortages of fresh water in some parts of the world, more flotation plants are using recycled or sea water for processing. Previous studies indicated that using water containing higher electrolyte concentrations improves the recovery of minerals by froth flotation. This has been attributed to the compression of the ionic diffuse layers around a particle and an air bubble (Wang and Peng,2014) as well as the inhibition of bubble coalescence in salt solutions (Craig et al.,1993).

As the mining of more disseminated ore deposits is predicted to increase in the future, a higher degree of particle grinding will be necessary to achieve liberation (Wightman et al.,2000), resulting in increasing amounts of fine and ultrafine particles making up the flotation feed. In recent years, a number of studies have documented a strong correlation between particle size and flotation recovery (Leistner et al.,2017; Jameson,2012; Leistner et al.,2016; Sivamohan,1990). According to Jameson,2012 and Trahar,1981, froth flotation is most efficient for particles ranging in size from 10-100 µm. Flotation recovery has been shown to decrease with increasing particle size (>100 µm), with this being attributed to a higher probability of particle-bubble detachments (Nguyen and Schulze,2003). On the other hand, if particles are too fine (<10 µm), flotation efficiency is limited by a smaller particle mass and its higher specific surface area (Lange et al.,1997). Small particle mass leads to a lower probability of particle-bubble collisions due to a lower momentum, and results in fine particles being recovered via entrainment rather than flotation by means of particle-bubble attachments (Lange et al.,1997). Higher surface area of fine particles has been associated with a more rapid reagent consumption compared to coarse particles, leading to a non-selective collection of fine particles and a reduction in the grade of the target mineral (Lange et al.,1997).

In a study by Leistner et al.,2017, the authors reported that the target particle-bubble ratio is not the sole parameter to govern flotation efficiency. It has been suggested that an increased number of fine and ultrafine gangue particles present in the feed can reduce the target particle-bubble collision efficiency, hence limiting the recovery of the target mineral. The aim of this current study was to examine these hypotheses by focusing on the interactions between coarse and fine galena and quartz particles during flotation in NaCl salt solutions. The recovery of galena was investigated by flotation experiments, measured zeta potentials as well as theoretical models representing the total free energy of the interaction for each condition. The outcome provides new insight into the recovery of galena via froth flotation in NaCl solutions, as a function of the target and gangue mineral particle size.

2. Experimental

2.1. Minerals and Reagents

The mineral chosen as the target was galena (PbS) with quartz (SiO_2) as the gangue mineral in the system. The galena sample was from an unknown location. The ICP-MS (Inductively Coupled Plasma Mass Spectrometry) analysis indicated that the galena sample contained 64.53% Pb (w/v).

The objective was to generate two size fractions for each mineral, a coarse (-75 + 53)μm and a fine (< 15) μm fraction. To do so, the galena and quartz samples were initially crushed using a jaw crusher. The crushed material was then combined with a NaCl salt solution (10 mM) and ground in a ball mill using zirconia media. Each sample was ground for a certain amount of time, before the mill was stopped, and a small sample of the pulp was removed for size analysis. Using a laser diffraction instrument (Microtrac S3500), the P_{50} (the size at which 50% of particles are passing) was measured. If the required particle size was not achieved, the mill was re started and the grinding carried on for a longer period of time. The grinding process continued till the desired particle size was achieved. Once this was done, the pulp was removed from the ball mill, and it was pressure filtered. The filtered sample was then sealed

inside a plastic bag, with no drying. This procedure was followed for both mineral samples. At the end, four separate fractions were produced, two for galena (coarse and fine) and two for quartz (coarse and fine). These four fractions were later used to generate the four feed particle systems in this study, namely: (CC) Coarse galena-Coarse quartz, (CF) Coarse galena-Fine quartz, (FC) Fine galena-Coarse quartz, and (FF) Fine galena-Fine quartz. All experiments were performed in deionised water containing either 10 mM or 100 mM sodium chloride (NaCl) of analytical grade. Analytical grade sodium hydroxide (NaOH) was used to regulate the solution pH. Analytical grade nitric acid (HNO_3) and hydrochloric acid (HCl) were used to make up the Aqua Regia solution.

2.2. Zeta Potential Measurements and the Charge Regulation at the Galena, Quartz and Air Bubble Surface Sites

Zeta potentials of galena and quartz particles were measured using a Malvern Nano-ZS90 zeta analyser (Malvern Instruments, UK) at room temperature. The measurements involved ultrafine (~5) µm galena or quartz particles dispersed in deionised water with a salt background of 10 mM NaCl, at a pH range of 2-10. At least 3 measurements were done at each condition, with the average values illustrated in Figure 3. These measured zeta potentials were used to determine the heterocoagulation tendency of galena and quartz particles during flotation as well as to calibrate the chemisorption models describing competitive ion binding at the galena and quartz surfaces.

Previous investigations indicated two separate binding sites on the surface of galena where the dissociation reactions take place, represented as: (1)- a negative galena site $\mathbf{X^-}$, where the protons (H^+) and the cations (Na^+) compete to bind directly to the site Eq.(1-2):

$$\mathrm{XH} \overset{\mathrm{pK_{H_1}}}{\Longleftrightarrow} \mathrm{X^-} + \mathrm{H^+} \quad (1)$$

$$\mathrm{XNa} \overset{\mathrm{pK_{Na}}}{\Longleftrightarrow} \mathrm{X^-} + \mathrm{Na^+} \quad (2)$$

and, (2)- a neutral galena site $\mathbf{X}$, where the protons (H^+) compete with the anions (Cl^-) for the site Eq.(3-4):

$$XH^{+} \overset{pK_{H_2}}{\Longleftrightarrow} X + H^{+} \quad (3)$$

$$XCl^{-} \overset{pK_{Cl}}{\Longleftrightarrow} X + Cl^{-} \quad (4)$$

Our chemisorption model for galena is a "two-site/not amphoteric" surface complexation model which assumes that there is only single-binding of ions at each of the sites.

In comparison, the process of ion competition taking place at the quartz surface site can be represented by the following dissociation reactions:

$$XH \overset{pK_H}{\Longleftrightarrow} X^{-} + H^{+} \quad (5)$$

$$XNa \overset{pK_{Na}}{\Longleftrightarrow} X^{-} + Na^{+} \quad (6)$$

The chemisorption model for quartz Eq.(5-6) is a "one-site/two pK" model, involving the competitive adsorption of protons (H^+) and cations (Na^+) at the negatively charged quartz sites, where only single binding of ions is involved.

The dissociation reactions taking place on air bubble surface sites are as follows:

$$XH \overset{pK_H}{\Longleftrightarrow} X^{-} + H^{+} \quad (7)$$

$$XH_2{}^{+} \overset{pK_{HH}}{\Longleftrightarrow} XH + H^{+} \quad (8)$$

$$XH - Cl^{-} \overset{pK_{HCl}}{\Longleftrightarrow} XH + Cl^{-} \quad (9)$$

The surface complexation model for an air bubble Eq.(7-9) is an amphoteric "one-site/two pK" model. The model indicates either a single binding Eq.(7) or a double-binding Eq.(8) of protons (H^+) at the negatively charged bubble site X^-. The anions (Cl^-) do not bind directly to a bubble site, rather they bind to a protonated site on the surface of the bubble Eq.(9).

It has been documented that an equilibrium between the adsorption and desorption of ions at specific surface sites can be used to determine the total surface charge (Hunter,1981). Governed by short-range molecular forces, each of the binding energies of the adsorption/desorption reactions is represented by an equilibrium constant K, or its counterpart pK = - log K. Here the terms pK_{H_1}, pK_{H_2} and pK_H are the equilibrium constants associated with the surface adsorption of protons. In this study the equilibrium constants for

the adsorption and desorption reactions of all ions were determined by least-square fitting to the measured zeta potentials and are presented in Tables 1-3.

Table 1. Parameters used to fit the chemisorption model for galena in NaCl salt solution (calibrated using the measured galena zeta potentials in 10 mM NaCl solution).

PARAMETER	VALUE
N_s negative (sites m^{-2})	1.519×10^{16}
N_s neutral (sites m^{-2})	2.765×10^{16}
pK_{H1}	5.265
pK_{H2}	2.393
pK_{Na}	-2.376
pK_{Cl}	7.911

Table 2. Parameters used to fit the chemisorption model for quartz (calibrated using the measured quartz zeta potentials in 10 mM NaCl solution). The values in the brackets are the ones previously reported in the literature (Chapel,1994; Davis et al.,1977).

PARAMETER	VALUE
N_s (sites m^{-2})	2.147×10^{16} ($0.5\text{-}5 \times 10^{16}$)
pK_H	5.652 (6.35)
pK_{Na}	3.093 (3.25)

Table 3. Parameters used to fit the chemisorption model for an air bubble calibrated using the measured bubble zeta potentials in 10 mM NaCl, taken from Yang et al.,2001.

PARAMETER	VALUE
N_s (sites m^{-2})	4.676×10^{16}
pK_H	5.812
pK_{HH}	2.984
pK_{HCl}	1.962

A phenomenon known as “charge regulation” was first described by Ninham and Parseginan in 1971. The authors indicated that the electrostatic potential, resulting from the overlapping diffuse parts of the double layers in conjunction with the localised concentration of ions, which varies with the changing separation distance between two interacting objects, is responsible for determining the total surface charge (Ninham and Parseginan,1971). The solution to the total surface charge is obtained by combining the Poisson-Boltzmann equation, which connects the electrostatic potential at any point in an electrolyte to the concentration of ions at that point (Pick,2015), to the individual adsorption/desorption reactions for the adsorbed ions within the Stern Layer (Zhao et al.,2015).

The total surface charge (σ_s) for a given site can be calculated according to:

$$\sigma_s = q_s N_s + \sum_i q_i \Gamma_i \tag{10}$$

where q_s is the charge of the dissociated site, N_s is the site density (number of sites per unit area) and q_i is the ionic charge (Parsons and Salis,2019).

The total amount of bound charge (Γ_i) from ion i can be calculated from:

$$\Gamma_i = \frac{N_s}{A_s}\left[\frac{a_i}{K_i} + \sum_j a_i a_j \left(\frac{1}{K_i K_{ij}} + \frac{1}{K_j K_{ji}}\right)\right] \tag{11}$$

where K_i and K_j indicate the single-binding of ion i and j, respectively, K_{ij} represents binding of ion j to a site with ion i already bound, and K_{ji} describes a site with ion i double-binding to a site with ion j already bound.

A_s is a measure of the total association or in other terms, an inverse of γ_s (γ_s being a fraction of fully dissociated surface sites) and can be written as:

$$A_s = \frac{1}{\gamma_s} = 1 + \sum_m \frac{a_m}{K_m}\left(1 + \sum_n \frac{a_n}{K_{mn}}\right) \quad (12)$$

142 The term a_i does not describe the surface activity of an ion, rather it corresponds to the
143 "partial ion activity" at a particular concentration, and according to Parsons and Salis,2015
144 and 2019, is quantified by:

$$a_i = c_i^{bulk} e^{-q_i\psi_0/kT} \quad (13)$$

145 where c_i^{bulk} is the concentration of ion i in the bulk, ψ_0 is the electrostatic potential at the
146 surface, k is the Boltzmann constant (1.3806 x 10^{-23} J/K) and T is the temperature (298 K).

147

148 2.3. Flotation Experiments

149 The flotation experiments were performed using an Agitair Model LA-500 flotation machine.
150 The four individually generated feed particle systems were tested: CC, CF, FC and FF. Each
151 experiment used ~ 50 grams of galena and ~50 grams of quartz particles, with the total solid
152 content being 10% (w/v). Test solutions were prepared using deionised water with either 10
153 mM or 100 mM NaCl, adjusted to pH 9, before the solids were introduced. The flotation
154 experiments were carried out in a one-litre cell with an impeller speed fixed at 1000 rpm. The
155 pulp was conditioned for 3 minutes before the air bubbles were introduced and kept at 4 L/min
156 for 7 minutes. Flotation concentrate was sampled at 7 minutes, at which point the experiment
157 was terminated. The concentrates and tailings were filtered, dried and weighed. A
158 representative sample was taken from each of the froth products, partially digested using the
159 Aqua Regia solution (HNO_3 + 3HCl) at 80°C for 1 hour, then appropriately diluted using
160 deionised water before its Pb content (% w/v) was determined by ICP-MS analysis.

161

162 2.4. Total Interaction Free Energy and the DLVO Theory

163 The DLVO theory describes the total interaction energy between two objects in terms of a
164 balance of the attractive and repulsive contributions to the total free energy. However, for NaCl

concentrations higher than 100 mM, the ionic diffuse layer force is screened, leaving the van der Waals force as the dominant factor in the interaction. The total interaction free energy (F_{tot}) can be broken down into four individual contributions:

$$F_{tot} = F_{el} + F_{en} + F_{vdW} + F_{chem} \quad (14)$$

F_{el} represents the direct electrostatic energy due to surface and electrolyte charges, F_{en} is the contribution due to the entropy (osmotic energy) of ions physisorbed near the surface. The term F_{vdW} represents the van der Waals interactions characterised by the Hamaker constant for the system and F_{chem} is the chemisorption free energy resulting from ion binding (Parsons and Salis,2019), also known as charge regulation. The electrostatic energy F_{el} is determined by the electrostatic potential $\psi(z)$ generated by physisorbed ions (the so-called electric double layer) and by the surface charge (Eq.10). Here, z represents the position of the ion (its distance from the galena surface) (Parsons and Ninham,2012):

$$F_{el} = \frac{\varepsilon_0 \varepsilon}{2} \int_0^L \left(\frac{d\psi}{dz}\right)^2 dz \quad (15)$$

and L represents the separation distance between the two interacting surfaces.

The entropic energy F_{en} is generated by the concentration profiles $c_i(z)$ of the adsorbed ions, according to the following:

$$F_{en} = kT \sum_i \int_0^L dz \left\{ c_i(z) \ln \frac{c_i(z)}{c_{i0}} - c_i(z) + c_{i0} \right\} \quad (16)$$

where c_{i0} is the bulk activity of ion i (Parsons and Ninham,2012). A more detailed description of the term F_{chem} from Eq.(14) can be found in the studies of Parsons and Salis,2015 and 2019.

While the chemisorption contributions to the total free energy are mainly influenced by the surface charge and the concentration and distribution of ions in the system, the non-electrostatic van der Waals interactions F_{vdW} are characterised by a Hamaker constant (A_{132}), with:

$$F_{vdW} = \frac{-A_{132}}{12\pi d^2} \quad (17)$$

The Hamaker constant characterises the interaction between sphere 1 and sphere 2 immersed in aqueous medium 3 (aqueous solution). Using Lifshitz theory, the Hamaker constant can be calculated from the frequency dependent dielectric properties (optical spectra) of the continuous phases (Lee and Singmund,2002; Bergström,1997). The non-retarded Hamaker constant (A_{132}) can be approximated as:

$$A_{132} = \frac{3kT}{2}{\sum_{n=0}^{\infty}}' \sum_{s=1}^{\infty} \frac{(\Delta_{13}\Delta_{23})^s}{s^3} \tag{18}$$

The prime on the first summation indicates that when n=0 (the static contribution) the value is multiplied by 0.5 (Takagishi et al.,2019).

The quantity in Eq.(18) is a reflection coefficient, defined as:

$$\Delta_{kl} = \frac{\varepsilon_k(i\zeta_m) - \varepsilon_l(i\zeta_m)}{\varepsilon_k(i\zeta_m) + \varepsilon_l(i\zeta_m)} \tag{19}$$

which describes the difference in the dielectric response function of material k and l, respectively. In Lifshitz theory, it is evaluated at the imaginary frequency $(i\zeta_m)$, where

$$\zeta_m = m\frac{4\pi^2 kT}{h} \tag{20}$$

Here h is the Planck constant (6.626 x 10^{-34} J/K), k is the Boltzmann constant, m is an integer (0,1,2,3,4…) and T is the absolute temperature. At room temperature, ζ_m are sampled at integral multiples of 2.4 x 10^{14} rad/s.

We apply a model for the dielectric function of galena provided by Bergström,1997, using:

$$\varepsilon(i\zeta_m) = 1 + \frac{C_{UV}}{1 + \left(\frac{\zeta_m}{\omega_{UV}}\right)^2} + \frac{C_{IR}}{1 + \left(\frac{\zeta_m}{\omega_{IR}}\right)^2} \tag{21}$$

Optical parameters $\mathbf{C_{UV}}$ and $\mathbf{C_{IR}}$ are the adsorption strengths in the UV and IR range, and for a cubic galena these values are 15.04 and 153, respectively. For a cubic galena, the terms $\boldsymbol{\omega_{UV}}$ and $\boldsymbol{\omega_{IR}}$, which represent the adsorption frequencies in the UV and the IR range, have a value of 0.167 (10^{16} rad/s) and 0.14 (10^{14} rad/s), respectively (Bergström,1997). The dielectric function of air is taken to be simply $\boldsymbol{\varepsilon_{air} = 1}$. The Hamaker constants for all the interactions presented in this study are calculated using the dielectric data for a cubic galena (Bergström,1997), for quartz (Chad and Richmond,1977) and for water (Fiedler et al.,2020), and are given in Table 4.

Table 4. The Hamaker constants (A_{132}) for the interactions in this study.

INTERACTION	$\mathbf{A_{132}}$ (J)
galena-water-galena	5.5693×10^{-20}
galena-water-quartz	2.9564×10^{-22}
galena-water-bubble	2.7741×10^{-21}
quartz-water-quartz	7.4508×10^{-21}
quartz-water-bubble	-1.0616×10^{-20}

The Debye length characterizes the screening distance of the electrostatic force, or in other words, the thickness of the electrical double layer denoted as (κ^{-1}), and is defined as:

$$\kappa^{-1} = \sqrt{\frac{\varepsilon_r \varepsilon_0 kT}{e^2 \sum_i \rho_i^{\infty} z_i^2}} \qquad (22)$$

where $\boldsymbol{\varepsilon_0}$ is the permittivity of free space, $\boldsymbol{\varepsilon_r}$ is the dielectric constant of the medium, $\mathbf{k}$ is the Boltzmann constant, $\mathbf{T}$ is the absolute temperature, $\mathbf{e}$ is the electronic charge, $\boldsymbol{\rho_i}$ is the number density of ion i and $\mathbf{z_i}$ is the ion valency. According to Eq.(22), the Debye length will decrease monotonically as the ion concentration increases and will continue to decrease to a point where no long-range electrostatic forces will be expected in a concentrated electrolyte (Smith et al.,2016).

2.4.1. The Poisson-Boltzmann model

The total free energy described by Eq.(14), develops as a result of ion adsorption (the electric double layer) at the surface, forming ion concentration profiles $\mathbf{c_i(z)}$. Ions adsorb primarily in response to the electrostatic potential $\boldsymbol{\psi(z)}$. Assuming that each ion is in equilibrium with the bulk solution, the concentration profile is formed as a Boltzmann distribution, determined by the electrostatic energy of the ion, according to:

$$c_i(z) = c_{i\infty}\exp\left(-\frac{Z_i e\psi(z)}{kT}\right) \tag{23}$$

where $\mathbf{k}$ is the Boltzmann constant, $\mathbf{T}$ is the temperature and $\mathbf{c_{i\infty}}$ is the bulk number concentration of all of the ions.

The electrostatic potential $\boldsymbol{\psi(z)}$ is determined by the Poisson equation (the first of Maxwell's equations):

$$\frac{d^2}{dz^2}\psi(z) = -\frac{e}{\varepsilon\varepsilon_0}\sum_i Z_i c_{i\infty}\exp\left(-\frac{Z_i e\psi(z)}{kT}\right) \tag{24}$$

where $\mathbf{e}$ is the elementary charge and $\mathbf{Z_i}$ is the valency of the corresponding ion. $\boldsymbol{\varepsilon}$ and $\boldsymbol{\varepsilon_0}$ are the dielectric constant of the medium and the permittivity of free space. Solving for $\mathbf{c_i(z)}$ and $\boldsymbol{\psi(z)}$ simultaneously, Eq.(23) and Eq.(24) together, form the nonlinear Poisson-Boltzmann (PB) model.

Solving the Poisson equation, Eq.(23), however, requires defining the boundary conditions relating the gradient of the electrostatic potential at the surfaces of the interacting objects, to their respective surface charges, as follows:

$$\left(\frac{d\psi}{dz^2}\right)_{surface} = \frac{-\sigma}{\varepsilon\varepsilon_0} \tag{25}$$

To do so, we apply the charge regulation model, Eq.(10), to determine the surface charges of the two surfaces. Here we solve the nonlinear Poisson-Boltzmann model by finite element

methods using the FEniCS software (Alnæs et al.,2015). Once $c_i(z)$ and $\psi(z)$ have been calculated, they are used to determine the total interaction free energy Eq.(14), between the two interacting objects, both represented as flat planes. Finally, the Derjaguin approximation (Derjaguin,1934) is applied to convert the flat-plane interaction energy $F(d)$ into a force $f(d)$ between the two spherical objects:

$$f(d) = 2\pi\left(\frac{R_1 R_2}{R_1 + R_2}\right)F(d) \tag{26}$$

where R_1 and R_2 are the radii of the two objects.

Figure 1 illustrates the sequence of steps required to perform the calculations presented in this study.

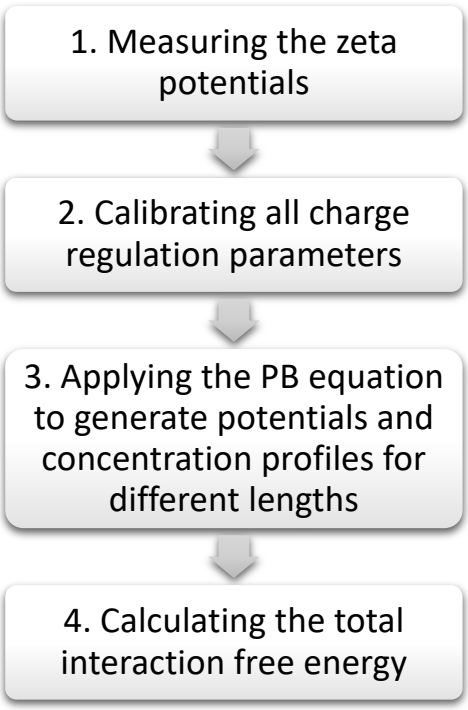

Figure 1. The calculation/optimization sequence implemented in the study.

1. Zeta potentials are measured as a function of pH and the ionic concentration.
2. The measured zeta potentials from Step 1 are used to calibrate the charge regulation parameters of our model, determining the charge-regulated surface charge (σ_s) in Eq.(10). The charge regulation parameters are fitted by least-square difference to minimize the difference between the measured zeta potentials and the surface potentials calculated by the PB model for galena, quartz and air bubble surfaces, separately.
3. Using the charge regulation parameters from Step 2 and the PB model described by Eq.(23) and Eq.(24), the potential and the ion concentration profiles for galena, quartz and air bubble interacting at various separation distances (d) are calculated.
4. Using the electrostatic potentials and the ion concentration profiles calculated in Step 3, the total interaction free energy between the two surfaces, separated by a distance (d), is calculated using Eq.(14). The total free energy between two flat surfaces is then converted to a force between spherical particles using the Derjaguin approximation Eq.(26).

3. Results and Discussion

3.1. Particle Size Distribution

Figure 2 illustrates the galena and quartz particle size distribution.

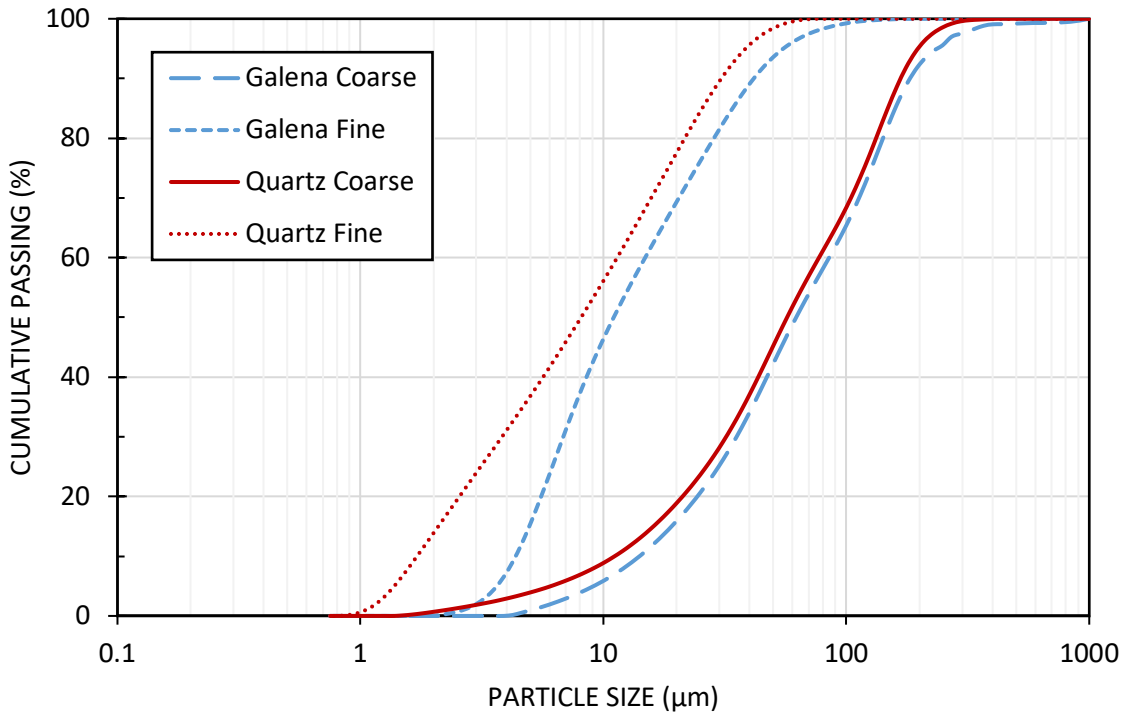

Figure 2. Galena and quartz particle size distribution curves for particles used to generate the four particle feed systems of the study.

For the purpose of calculating the total interaction free energy for each system, the P_{50}, which represents the size at which 50% of particles are passing, was used. The following particle diameters were used in all calculations: Coarse galena = 62.23µm, Fine galena = 11.03µm, Coarse quartz = 57.05µm, Fine quartz = 8.10µm.

3.2. Zeta Potential Analysis

Figure 3 illustrates the measured and calculated zeta potentials of galena and quartz as a function of pH with 10 mM NaCl used as the background electrolyte solution.

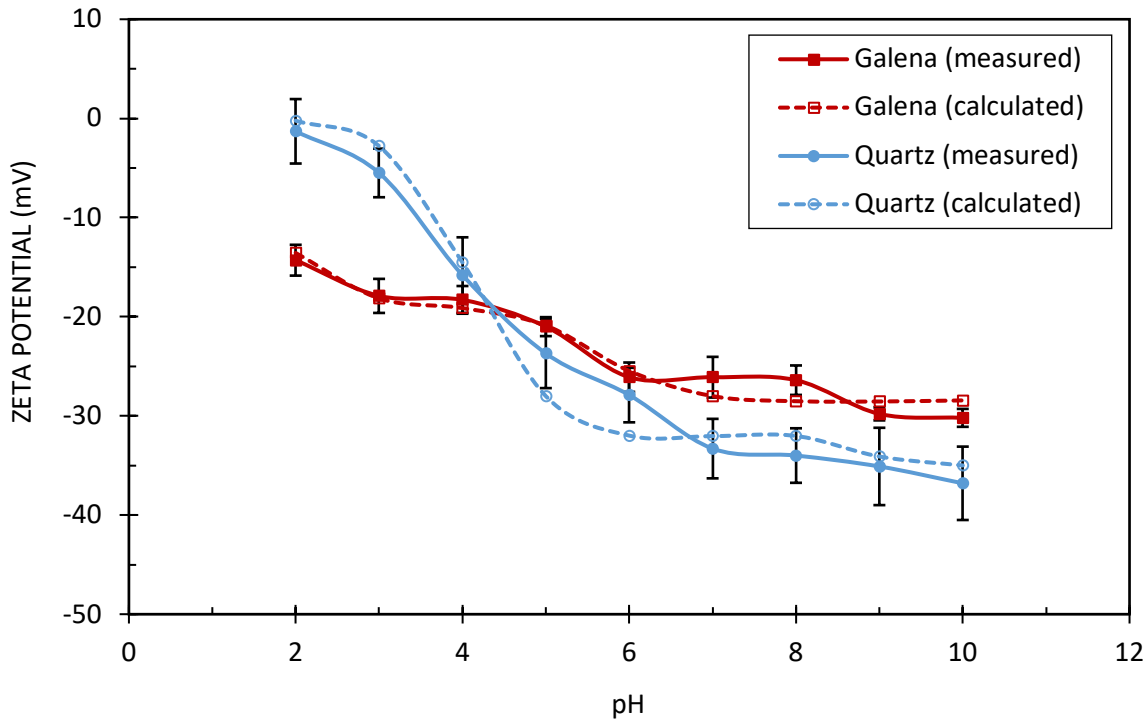

Figure 3. Influence of pH on the zeta potentials of galena and quartz particles measured in 10 mM NaCl salt solution (solid lines) and the zeta potentials of galena and quartz calculated using the charge regulation models for galena and quartz (broken lines).

The measured zeta potentials of galena in 10 mM NaCl background solution indicated a negatively charged surface over the investigated pH range, decreasing from -14 mV to -30 mV as the pH increased from 2 to 10. The zeta potentials of quartz also showed a negatively charged surface for the pH range tested, from decreasing -1 mV to -37 mV as the pH was increased from 2 to 10. The quartz zeta potentials were consistent with the values previously reported by Liang et al., 2017.

A smaller difference between two particles' zeta potentials implies reduced coagulation, resulting from a decrease in electrostatic attraction between the particles (Mitchell et al.,2005; Xu et al.,2012). From the results in Figure 3, at an alkaline pH (pH 9), the difference in the galena and quartz zeta potentials is reasonably small, and for this reason pH 9 was chosen for the micro-flotation experiments.

280 Figure 4 shows the measured and calculated zeta potentials of an air bubble in 1 mM and 10
281 mM NaCl solutions, as a function of pH. The measured zeta potentials were taken from a study
282 by Yang et al.,2001.

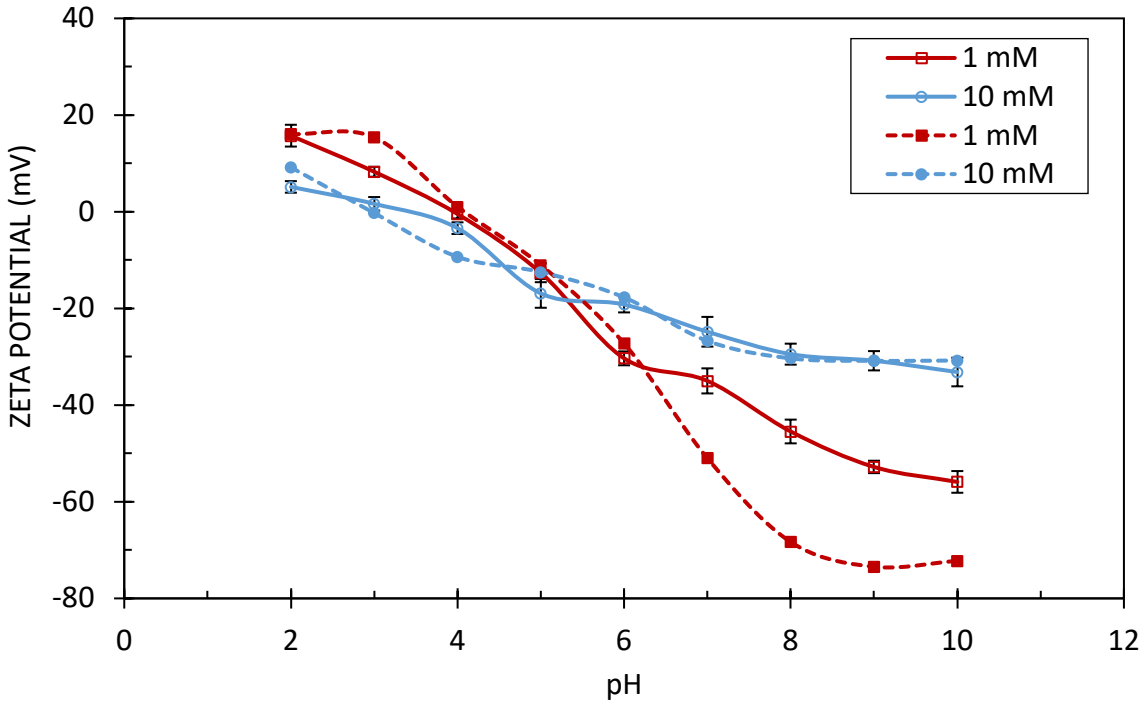

Figure 4. Zeta potential versus pH curves for an air bubble conditioned in 1 mM and 10 mM of NaCl salt solutions. Solid lines represent the measured values (taken from a study by Yang et al.,2001), the broken lines illustrate the calculated values using the chemisorption model for the air bubble.

283 At the lower ionic concentration of 1 mM NaCl, the bubble zeta potentials decrease from +16
284 mV to -56 mV as the pH increases from 2 to 10. At 10 mM NaCl, the bubble zeta potentials
285 decrease from +5 mV to -33 mV, as the pH increases from 2 to 10. The results in Figure 4 show
286 that an air bubble is positively charged at pH 2-3, with the exact zeta potential value depending
287 on the NaCl concentration.

3.3. Flotation Experiments

The recovery of galena after flotation in 10 mM and 100 mM NaCl salt solutions at pH 9, as a function of the four feed particle systems is shown in Figure 5.

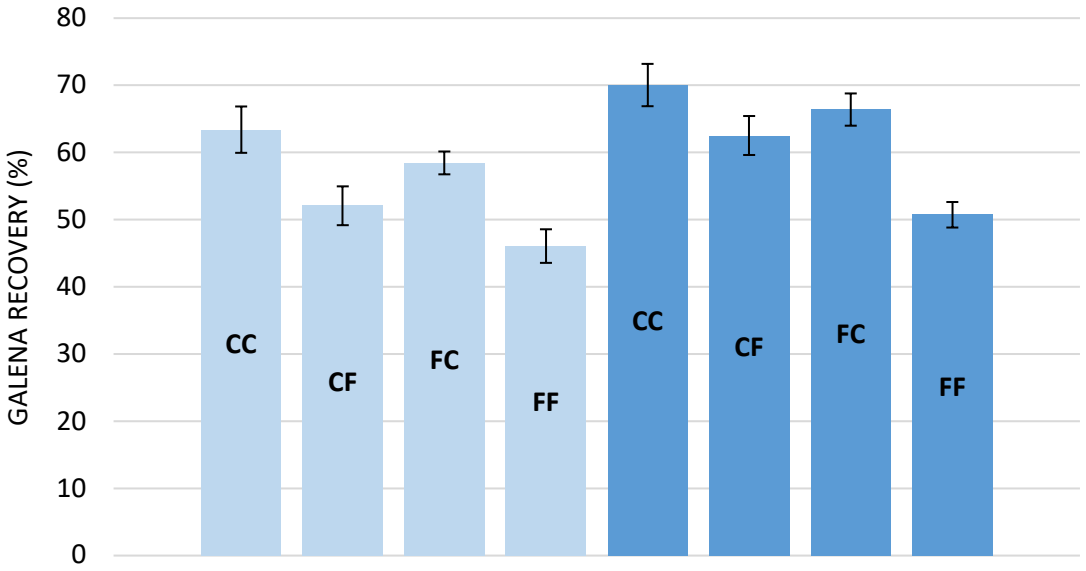

Figure 5. The recovery of galena (%) from the flotation experiments conducted in 10 mM (light blue) and 100 mM (dark blue) NaCl salt solutions at pH 9, as a function of the four feed particle systems. **(CC):** **C**oarse galena/**C**oarse quartz, **(CF):** **C**oarse galena/**F**ine quartz, **(FC):** **F**ine galena/**C**oarse quartz, and **(FF):** **F**ine galena/**F**ine quartz.

The results from Figure 5 suggest that an increase in NaCl concentration in solution from 10 mM to 100 mM increases the recovery of galena. When looking at the individual particle systems, the CC particle system produced the highest galena recovery of ~ 63% in 10 mM and ~70% in 100 mM NaCl salt solution. This finding does not come as a surprise considering the size of the galena particles making up the feed was within the optimum particle size range for flotation reported by Jameson,2012 and Trahar,1981. The lowest galena recovery of ~46% in 10 mM and ~50% in 100 mM NaCl salt solution for the FF particle system, could be attributed to a lower target particle-bubble collision efficiency due to a lower mass of the galena particles.

The low galena recovery in the FF particle system might have also resulted from a higher water recovery and a higher number of gangue (quartz) particles reporting to the froth product.

The effects on flotation efficiency of using coarse and fine particles as feed have been studied and discussed in detail in the literature (Lange et al.,1997; Jameson,2012; Leistner et al.,2017; Nguyen and Schulze,2003, Yao et al.,2018). However, the current collision efficiency models do not explain the flotation results for the CF and FC particle systems. Shown in Figure 5, the recovery of galena in the CF particle system was ~52% in 10 mM and ~62% in 100 mM NaCl, compared to ~58% and ~66% for the FC particle system in 10 mM and 100 mM NaCl, respectively. These results demonstrate that the size of the gangue (quartz) particles in the feed affects the recovery of the target (galena) mineral which is in agreement with the findings previously reported by Leistner et al.,2017. The lower galena recovery in the CF particle system can possibly be attributed to a greater number of individual fine quartz particles in the feed, which resulted from a higher degree of particle liberation required to generate a fine quartz fraction. These quartz particles are hydrophilic in nature, therefore, having an increased number of them in the feed will negatively impact galena recovery, as shown in Figure 5.

3.4. Total Interaction Free Energy

The calculated total interaction free energies between coarse and fine galena and quartz particles in 10 mM and 100 mM NaCl salt solutions, at pH 9 are illustrated in Figures 6 and 7.

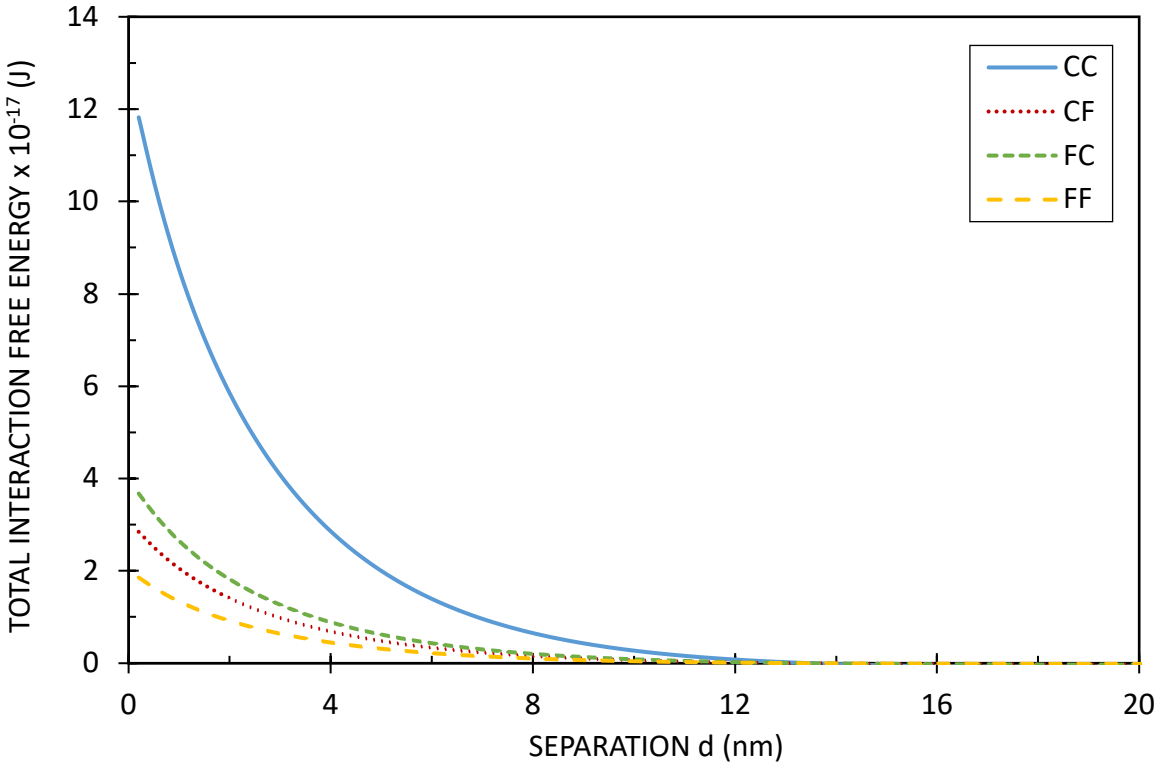

Figure 6. The total interaction free energy versus the separation distance between galena and quartz particles for the four different feed particle systems in 10 mM NaCl salt solution, at pH 9. **CC=C**oarse galena/**C**oarse quartz, **CF=C**oarse galena/**F**ine quartz, **FC=F**ine galena/**C**oarse quartz, and **FF=F**ine galena/**F**ine quartz.

The results in Figure 6 show that in all four galena/quartz particle systems repulsion dominates the interactions at separations of < 12 nm. The CC particle system has the highest energy barrier of 12 x 10^{-17} J. This large energy barrier for the CC particle system suggests that it will be more difficult for coarse galena and coarse quartz particles to aggregate due to a high electrostatic repulsion acting between them. In the context of froth flotation, a larger repulsive barrier between galena and quartz gives rise to conditions which help to increase galena recovery. This is consistent the results from the flotation experiments in Figure 5. In terms of competitive ion binding at the surface sites, in the CC particle system where each individual galena and quartz particle has a larger surface area, a stronger repulsion dominates the interaction due to a higher number of surface sites available for ion adsorption.

The lowest energy barrier of around 2 x 10^{-17} J is reported for the FF particle system. This finding implies that there is a higher probability of fine galena/fine quartz particle agglomeration,

caused by a lower electrostatic repulsion between these particles. The results from the flotation experiments in Figure 5 are in agreement with this theoretical prediction.

The energy profiles for the CF and the FC particle systems also indicate the presence of an energy barrier of 3 x 10^{-17} J and 4 x 10^{-17} J, respectively. A significantly lower repulsion is noticed in these two particle systems compared to the CC particle system. In Figure 6, the energy barrier for the FC particle system is 3 times lower than the energy barrier for the CC system, yet the flotation results for the FC system indicated a galena recovery of around 58%, only slightly less than that for the CC system, of around 63%. These experimental results together with the theoretical predictions suggest that despite a reduced repulsion between fine galena and coarse quartz particles, the overall recovery of galena is not jeopardised.

The total interaction free energies between galena and quartz particles for the four particle systems in 100 mM NaCl salt solution, at pH 9, are given in Figure 7.

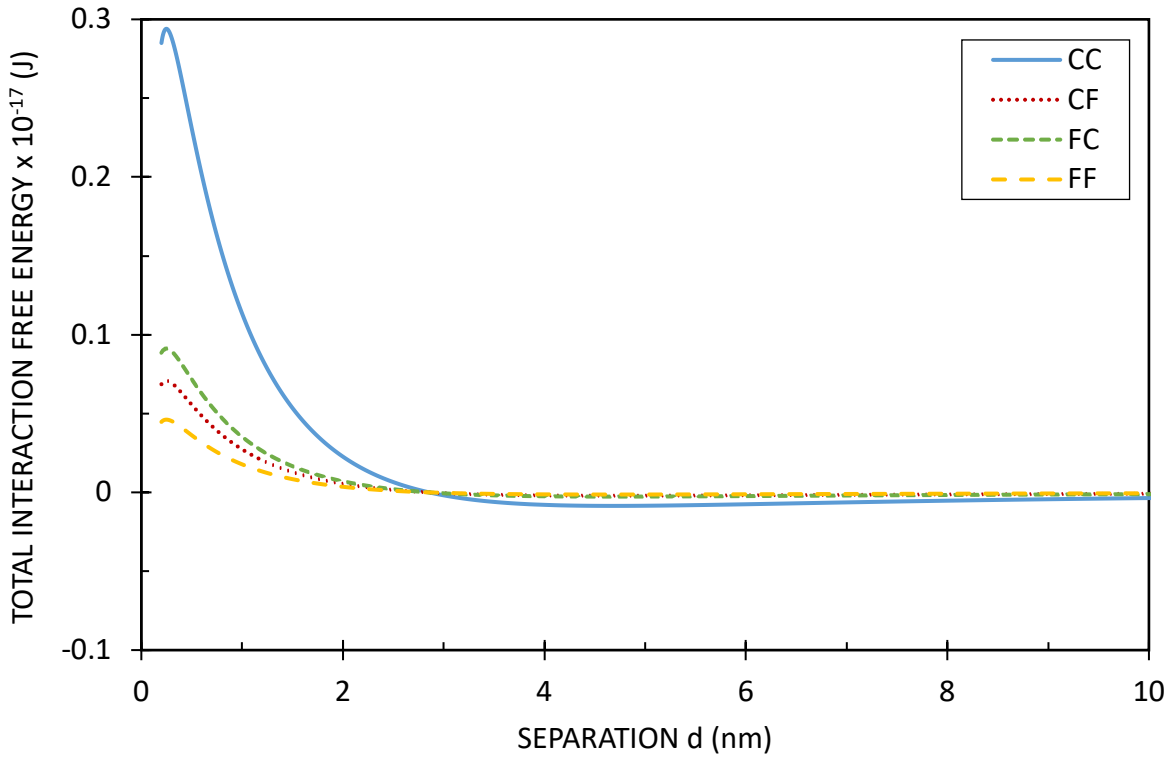

Figure 7. The total interaction free energy versus the separation distance between galena and quartz particles for the four different feed particle systems in 100 mM NaCl salt solution, at pH 9. **CC=C**oarse galena/**C**oarse quartz, **CF=C**oarse galena/**F**ine quartz, **FC=F**ine galena/**C**oarse quartz, and **FF=F**ine galena/**F**ine quartz.

342 The energy curves for the four particle systems in Figure 7 illustrate an electrostatic repulsion
343 as the dominating interaction in all systems. The main difference between the energy
344 interactions in 10 mM NaCl (Figure 6) and the interactions in 100 mM NaCl (Figure 7) is the
345 magnitude of the repulsion between galena and quartz particles. An increase in the ionic
346 concentration shortens the screening distance and results in significantly less energy required
347 to form an attachment between galena and quartz particles. According to the chemisorption
348 model for galena Eq.(1-4) and the galena zeta potentials from Figure 4, it is the anions (Cl^-)
349 present in the system which predominantly regulate the charge on the galena surface,
350 indicated by the large coefficient (pK_{Cl}=7.911) for chloride ion binding on the galena surface
351 sites. Effectively, the addition of NaCl salt ions will make the surface of galena more negatively
352 charged. On the other hand, in the chemisorption model for quartz, the anion (Cl^-) binding is
353 not taken into consideration as the negatively charged quartz surface will tend to oppose the
354 direct adsorption of an anion on its surface sites. Only the cation (Na^+) binding taking place on
355 the quartz surface sites is considered. An increase in the NaCl salt ion concentration in the
356 system will, therefore, neutralise the surface of a quartz particle. The results from the flotation
357 experiments indicated a higher galena recovery in 100 mM NaCl compared to 10 mM NaCl salt
358 solution for each particle system.

359 Figure 8 shows the total interaction energies between two galena particles of different sizes, in
360 10 mM (left) and 100 mM (right) NaCl salt solutions, at pH 9.

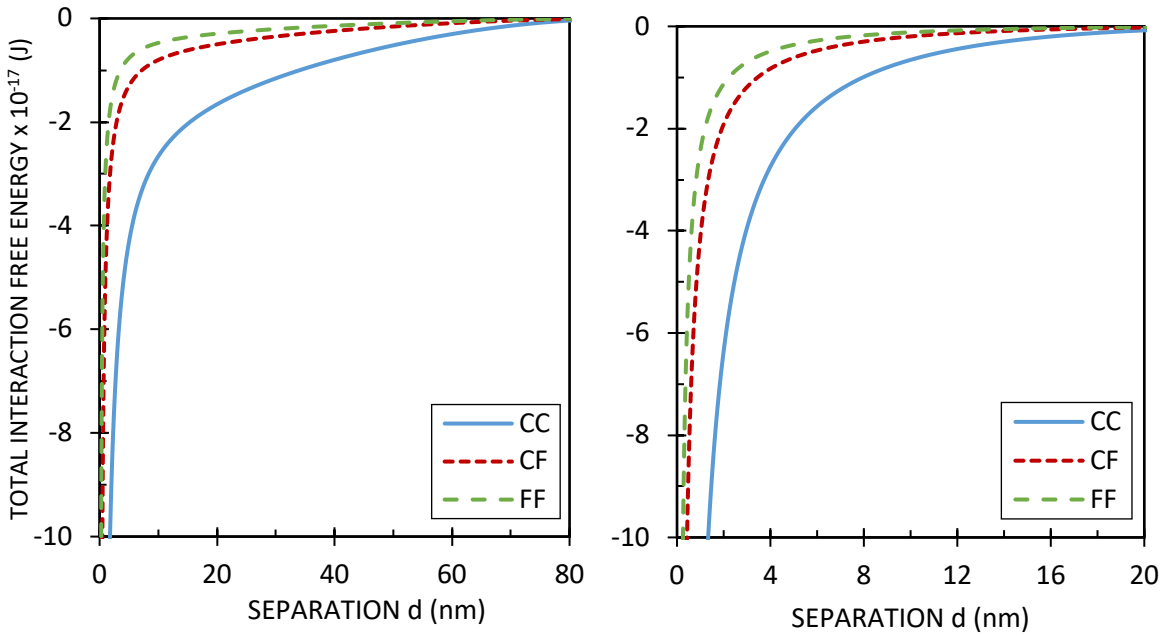

Figure 8. The total interaction free energy versus the separation distance between two galena particles in 10 mM (left) and 100 mM (right) NaCl salt solutions, at pH 9. **CC=C**oarse galena/**C**oarse galena, **CF=C**oarse galena/**F**ine galena and **FF=F**ine galena/**F**ine galena.

The energy curves representing galena/galena interactions show an attraction as the dominating force between the two particles, irrespective of their size or the ionic concentration of solution. This attraction extends over a much longer separation distance of ~80nm in 10 mM compared to ~20nm in 100 mM NaCl salt solution. The galena particles involved in the coarse/fine (CF) and the fine/fine (FF) interactions need to be closer than for the other systems before they aggregate.

The total interaction free energies between two quartz particles of various sizes were also evaluated and are presented in Figure 9, with the energy curves in 10 mM NaCl on the left and the energy curves in 100 mM NaCl salt solutions on the right.

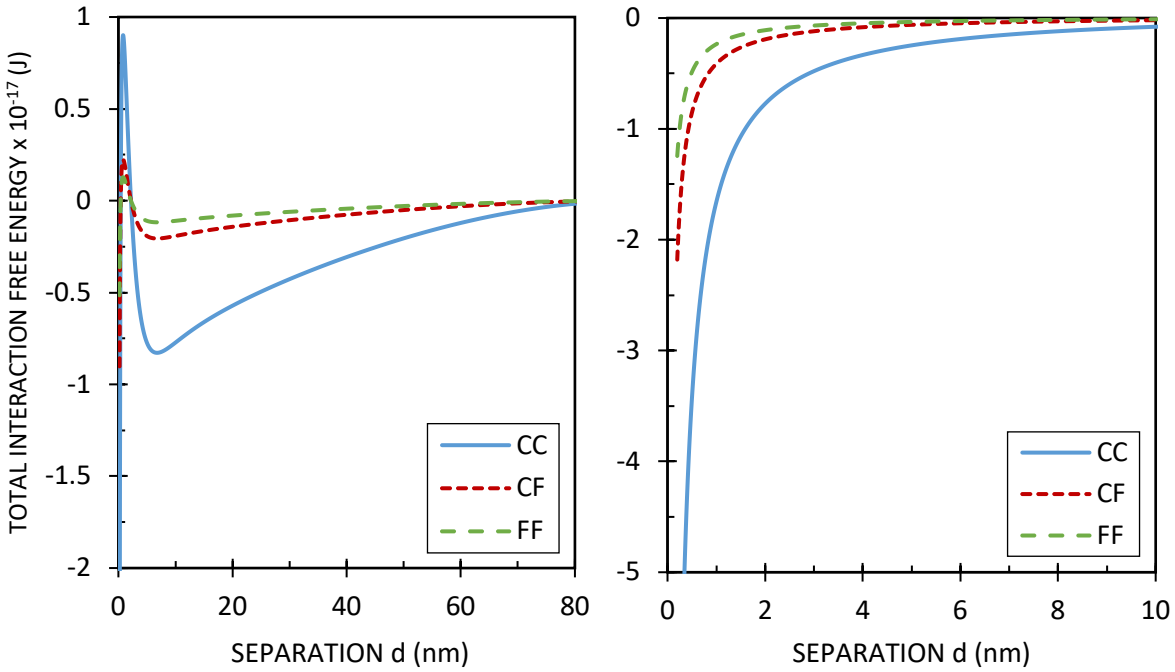

Figure 9. The total interaction free energy versus the separation distance between two quartz particles in 10 mM (left) and 100 mM (right) NaCl salt solutions, at pH 9. **CC=C**oarse quartz/**C**oarse quartz, **CF=C**oarse quartz/**F**ine quartz and **FF=F**ine quartz/**F**ine quartz.

An energy barrier appears for all interactions in Figure 9 (left), and is highest for the two coarse quartz particles (CC) and lowest for the two fine quartz particles (FF). The appearance of the energy barrier suggests that electrostatic repulsion is stronger than attraction between the two quartz particles. A second minimum energy is observed for the quartz/quartz interactions in 10 mM NaCl, with the lowest energy for the CC interaction. As the distance of separation between the two coarse quartz particles reduces from ~80 nm to ~5 nm, attraction increases. For distances of separation <5 nm, an increasing electrostatic repulsion, due to the overlapping of the diffuse double layers, acts as an energy barrier.

The quartz/quartz interactions in 100 mM NaCl salt solution (Figure 9, right) all indicate attraction as the dominating force acting between the two quartz particles. This implies that an increase in ionic concentration from 10 mM to 100 mM will facilitate quartz/quartz aggregation.

Figure 10 shows the total interaction free energies calculated between coarse/fine galena particles and an air bubble in 10 mM (left) and 100 mM (right) NaCl salt solutions, at pH 9.

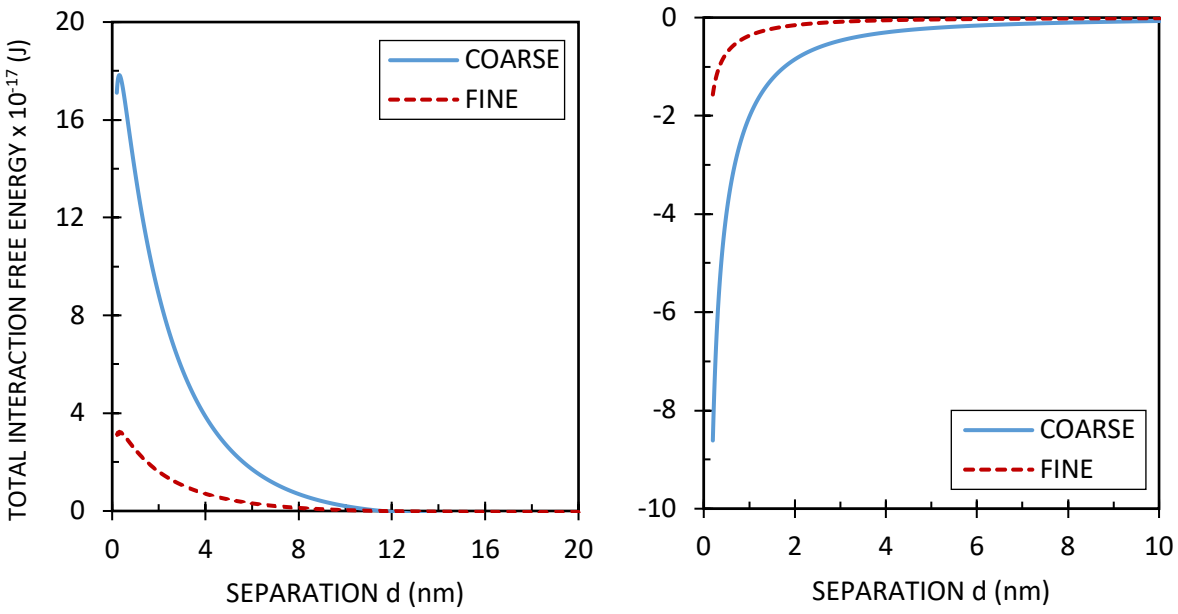

Figure 10. The total interaction free energy versus the separation distance between galena and air bubble in 10 mM (left) and 100 mM (right) NaCl salt solutions, at pH 9, as a function of galena particle size.

At the lower NaCl concentration (Figure 10, left) the interaction between a coarse galena particle and an air bubble is dominated by a strong repulsion at distances of separation <20nm. The coarse galena/air bubble interaction displays a significantly higher energy barrier of 18 x 10^{-17} J compared to the fine galena/air bubble energy barrier of around 4 x 10^{-17} J, suggesting that an attachment between a fine galena particle and air bubble is more probable.

At the higher NaCl concentration of 100 mM in Figure 10 (right), the attractive forces dominate the coarse and fine galena interactions with the air bubble. In the context of froth flotation, this attraction at the higher ionic concentration is favourable. It signifies that, irrespective of the galena particle size, galena/air bubble interactions should result in stable attachments.

Figure 11 illustrates the total interaction free energies calculated between coarse/fine quartz particles and an air bubble in 10 mM (left) and 100 mM (right) NaCl salt solutions, at pH 9.

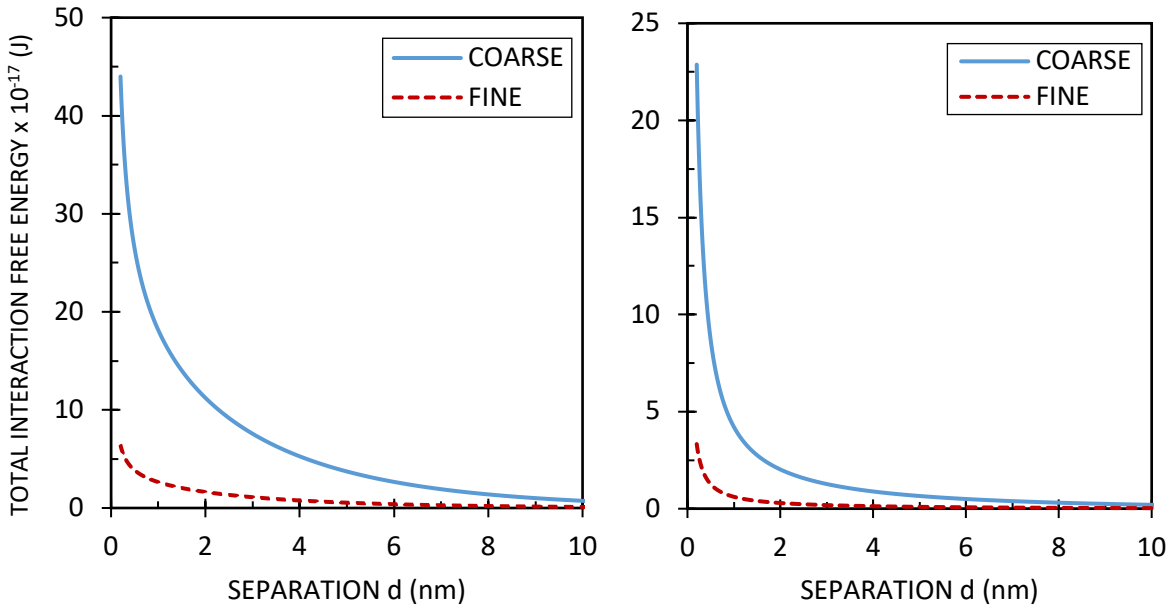

Figure 11. The total interaction free energy versus the separation distance between quartz and air bubble in 10 mM (left) and 100 mM (right) NaCl salt solutions, at pH 9, as a function of quartz particle size.

Figure 11 (left and right), show quartz/air bubble interactions which are dominated by strong repulsion at both NaCl concentrations. The coarse quartz/air bubble interaction curves show higher energy barriers (45 x 10^{-17} J for 10 mM and 22 X 10^{-17} J for 100 mM) compared to the fine quartz/air bubble interaction curves which shows 5 x 10^{-17} J and 2.5 x 10^{-17} J for 10 mM and 100 mM NaCl, respectively.

The theoretical predictions in Figure 11 suggest that even when the ionic concentration in solution is increased, the interaction of a quartz particle with an air bubble is always repulsive. This repulsion decreases for the higher NaCl concentration, but, based on the theoretical predictions presented in this study, air bubbles are still more likely to form an attachment with the galena particles (Figure 10) than with the quartz particles (Figure 11). On the basis of the total interaction free energy calculations, the higher recovery reported for the FC particle system in Figure 5 could be attributed to the aggregation of the fine galena particles, or in other words, fine galena particles forming “particle clusters”, shown by a dominating attraction between the two fine galena particles in Figure 8. We presume that these galena “particle clusters” would behave in a similar fashion to the coarse galena particles, in the way they are recovered. The CF particle system, on the other hand, is characterised by a repulsion between

411 the fine quartz particles, suggesting that these are being recovered as individual fine quartz
412 particles, and not as aggregates. An interesting point to mention relating to the CF particle
413 system, is that in 10 mM NaCl salt solutions, it is the fine quartz and not the coarse galena
414 particle which has a lower repulsion towards an air bubble.

415

416 4. Conclusion

417 In this study we have investigated the interactions of coarse and fine galena and quartz
418 particles and their implications for flotation in NaCl salt solutions. Four different galena/quartz
419 particle systems were tested: 1. (CC) Coarse galena/Coarse quartz, 2. (CF) Coarse galena/Fine
420 quartz, 3. (FC) Fine galena/Coarse quartz and 4. (FF) Fine galena/Fine quartz. Our results
421 showed that the CC particle system produced the highest galena recovery, while the FF particle
422 system produced the lowest recovery. Our results also indicated that the recovery of galena
423 improved in the higher NaCl concentration.

424 The flotation experiments on the mixed galena/quartz particle systems (CF and FC) showed
425 that the recovery of galena is affected by the size of the gangue (quartz) particles in the feed. It
426 was shown that if the size of the quartz particles was increased, the recovery of fine galena
427 improved. We discussed these results in terms of the competitive ion binding described by the
428 chemisorption models for galena, quartz and air bubble as well as the theoretical models
429 representing the interactions for each tested condition. We found that these models provided
430 a plausible explanation for the results from the flotation experiments.

431 This study presents new findings on the interactions of coarse and fine particles in a flotation
432 system, which can aid in the interpretation of observed behaviour in other flotation systems.
433 Nonetheless, the interactions involving systems with fine and coarse particles with different
434 surface properties still require more investigating before they can be integrated into the
435 currently established efficiency modelling approaches.

5. References

Alnæs, M., Blechta, J., Hake, J., Johansson, A., Kehlet, B., Logg, A., Richardson, C., Ring, J., Rognes, M.E. and Wells, G.N. The FEniCS Project Version 1.5. Archive of Numerical Software, Vol.3 No.100, 2015.

Bergström, L. (1997). Hamaker constants of inorganic materials. *Advances in Colloid and Interface Science* ***70,*** 125-169.

Chan, D. and Richmond, P. (1977). Van der Waals forces for mica and quartz: calculations from complete dielectric data. *Proceedings of the Royal Society. Lond. A* ***353*** *(1673),* 163-176.

Chapel, J.-P. (1994). Electrolyte species dependent hydration forces between silica surfaces. *Langmuir* ***10,*** 4237-4243.

Craig, V.S.J., Ninham, B.W. and Pashley, R.M. (1993). The effect of electrolytes on bubble coalescence in water. *The Journal of Physical Chemistry* ***97*** *(39),* 10192-10197.

Davis, J.A., James, R.O. and Leckie, J.O. (1977). Surface Ionization and Complexation at the Oxide/Water Interface. *Journal of Colloid and Interface Science* ***63*** *(3),* 480-499.

Derjaguin, B. (1934). Untersuchungen über die Reibung und Adhäsion, IV. *Kolloid-Zeitschrift* ***69***, 155-164.

Fiedler, J., Boström, M., Persson, C., Brevik, I., Corkery, R., Buhmann, S.Y. and Parsons, D.F. (2020). Full-spectrum High-resolution modelling of the dielectric function of water. *The Journal of Physical Chemistry B* ***124*** *(15),* 3103-3113.

Hunter, R.J. (1981). Zeta Potential in Colloid Science: Principles and Applications. Academic Press.

Jameson, G.J. (2012). The effect of surface liberation and particle size on flotation rate constants. *Minerals Engineering* ***36-38,*** 132-137.

Lange, A.G., Skinner, W.M. and Smart, R.St.C. (1997). Fine:Coarse particle interactions and aggregation in sphalerite flotation. *Minerals Engineering* ***10*** *(7),* 681-693.

461 Lee, S. and Sigmund, W.M. (2002). AFM study of repulsive van der Waals forces between Teflon
462 AF™ thin film and silica or alumina. *Colloids and Surfaces A: Physicochemical and*
463 *Engineering Aspects* ***204,*** 43-50.

464 Leistner, T., Embrechts, M., Leißner, T., Chehreh Chelgani, S., Osbahr, I., Möckel, R., Peuker, U.A.
465 and Rudolph, M. (2016). A study of the reprocessing of fine and ultrafine cassiterite from
466 gravity tailing residues by using various flotation techniques. *Minerals Engineering* ***96-***
467 ***97,*** 94-98.

468 Leistner, T., Peuker, U.A. and Rudolph, M. (2017). How gangue particle size can affect the
469 recovery of ultrafine and fine particles during froth flotation. *Minerals Engineering* ***109,***
470 1-9.

471 Liang, L., Wang, L., Nguyen, A.V. and Xie, G. (2017). Heterocoagulation of alumina and quartz
472 studied by zeta potential distribution and particle size distribution measurements.
473 *Powder Technology* ***309,*** 1-12.

474 Mitchell, T.K., Nguyen, A.V., Evans, G.M. (2005). Heterocoagulation of chalcopyrite and pyrite
475 minerals in flotation separation. *Advances in Colloid and Interface Science* ***114-115,*** 227-
476 237.

477 Nguyen, A.V. and Schulze, H.-J. (2003). Colloidal Science of Flotation. Marcel Dekker Inc., New
478 York.

479 Ninham, B.W. and Parsegian, V.A. (1971). Electrostatic potential between surface bearing
480 ionizable groups in ionic equilibrium with physiologic saline solution. *Journal of*
481 *Theoretical Biology* ***31*** *(3),* 405-428.

482 Parsons, D.F. and Ninham, B.W. (2012). Nonelectrostatic ionic forces between dissimilar
483 surfaces: A mechanism for colloid separation. *The Journal of Physical Chemistry C* ***116,***
484 7782-7792.

485 Parsons, D.F. and Salis, A. (2015). The impact of the competitive adsorption of ions at surface
486 sites on surface free energies and surface forces. *The Journal of Chemical Physics* ***142.***

Parsons, D.F. and Salis, A. (2019). A thermodynamic correction to the theory of competitive chemisorption of ions at surface sites with nonelectrostatic physisorption. *The Journal of Chemical Physics* ***151****.*

Pick, C. (2015). Electrical double layer interactions with surface charge heterogeneities. PhD Thesis. Johns Hopkins University. Baltimore, Maryland.

Sivamohan, R. (1990). The problem of recovering very fine particles in mineral processing-a review. *International Journal of Mineral Processing* ***28*** *(3-4),* 247-288.

Smith, A.M., Lee, A.A. and Perkin, S. (2016). The electrostatic screening length in concentrated electrolytes increases with concentration. *Journal of Physical Chemistry Letters* ***7,*** 2157-2167.

Takagishi, H., Masuda, T., Shimoda, T., Maezono, R. and Hongo, K. (2019). Method for the calculation of the Hamaker constants of organic materials by the Lifshitz macroscopic approach with Density Functional Theory. *The Journal of Physical Chemistry* ***123,*** 8726-8733.

Trahar, W.J. (1981). A rational interpretation of the role of particle size in flotation. *International Journal of Mineral Processing* ***8,*** 289-327.

Wang, B. and Peng, Y. (2014). The effect of saline water on mineral flotation – A critical review. *Minerals Engineering* ***66-68,*** 13-24.

Wightman, E.M., Grano, S.R. and Ralston, J. (2000). Selectivity in the polymer assisted separation of galena from quartz by flotation. *Minerals Engineering* ***13*** *(8-9),* 843-856.

Xu, D., Ametov, I. and Grano, S.R. (2012). Quantifying rheological and fine particle attachment contributions to coarse particle recovery in flotation. *Minerals Engineering* ***39,*** 89-98.

Yang, C., Dabros, T., Li, D., Czarnecki, J. and Masliyah, J.H. (2001). Measurement of the Zeta Potential of Gas Bubbles in Aqueous Solutions by Microelectrophoresis. *Journal of Colloid and Interface Science* ***243,*** 128-135.

512 Yao, J., Xue, J., Li, D., Fu, Y., Gong, E. and Yin, W. (2018). Effects of fine-coarse particles
513 interaction on flotation separation and interaction energy calculation. *Particulate*
514 *Science and Technology* ***36*** *(1),* 11-19.

515 Zhao, C., Ebeling, D., Siretanu, I., van den Ende, D. and Mugele, F. (2015). Extracting local surface
516 charges and charge regulation behaviour from atomic force microscopy
517 measurements at heterogeneous solid-electrolyte interfaces. *Nanoscale* ***7,*** 16298-
518 16311.